Available online at www.sciencedirect.com
ScienceDirect
Journal of Computational Physics 227 (2008) 5671–5690
JOURNAL OF COMPUTATIONAL PHYSICS
www.elsevier.com/locate/jcp

# An investigation into curved and moving boundary treatments in the lattice Boltzmann method

P.-H. Kao, R.-J. Yang *

*Department of Engineering Science, National Cheng Kung University, 1 University Road, Tainan 70101, Taiwan*

Received 18 May 2007; received in revised form 15 October 2007; accepted 4 February 2008
Available online 15 February 2008

**Abstract**

Curved boundary treatments provide a means of improving the computational accuracy of the conventional stair-shaped approximation used in lattice Boltzmann (LB) simulations. Furthermore, curved boundary treatments can be extended to the modeling of moving boundary problems simply by adding a momentum term to the bounced distribution functions at the solid surface. This study commences by investigating three conventional interpolating treatments for curved boundaries in LB problems, namely the Filippova and Hänel (FH) model [O. Filippova, D. Hänel, Grid refinement for lattice-BGK models, J. Comput. Phys. 147 (1998) 219–228], Bouzidi's model [M. Bouzidi, M. Firdaouss, P. Lallemand, Momentum transfer of a Boltzmann-lattice fluid with boundaries, Phys. Fluids 13(11) (2001) 3452–3459], and Yu's model [D. Yu, R. Mei, W. Shyy, A Unified Boundary Treatment in Lattice Boltzmann Method, AIAA 2003-0953, New York, 2003]. Previous investigations have indicated that the interpolations would break the mass conservation at the boundaries, since the inaccuracy in evaluation of the momentum transfer at boundary leads to a net mass flux. Based on this reason, a concept of the interpolation-free treatment for modeling the curved and moving boundary conditions is proposed to overcome the drawback of these interpolation-based curved boundary treatments. In present study, two interpolation-free models are then proposed, namely on-site interpolation-free (OSIF) and composite interpolation-free (CPIF) models. These proposed models are initially applied to simulate the flow in the channels containing a stationary square block positioned at various locations along the longitudinal axis. The simulations results are then compared with those obtained using the three conventional interpolating treatments. The interpolation-free models are then applied to the case of moving boundary problems in which a square block and a cylindrical block, respectively, move with a constant speed along a channel containing stationary flows. To test the Galilean effect of the proposed CPIF model, a Couette flow past the stationary square/cylinder block with the moving top/bottom walls is simulated. Overall, the numerical results show that the proposed interpolation-free curved treatment models significantly improve the accuracy of the mass flux computation near the solid surface, and thus enhance the accuracy of the momentum interaction at the moving boundaries.


*Keywords:* Lattice Boltzmann method (LBM); Curved boundary; Moving boundary; Interpolation

* Corresponding author. Tel.: +886 6 200 2724; fax: +886 6 276 6549.
*E-mail address:* rjyang@mail.ncku.edu.tw (R.-J. Yang).

0021-9991/$ - see front matter © 2008 Elsevier Inc. All rights reserved.
doi:10.1016/j.jcp.2008.02.002

## 1. Introduction

The lattice Boltzmann method (LBM) is a powerful numerical technique for simulating fluid flows and modeling the physics in fluids [1–4]. The LBM is based on kinetic theory by using the particles distribution functions and is modeled on uniform Cartesian lattices with diagonal links (directions) in space as a consequence of the discrete velocity sets. In LB simulations, collision and propagation routines are performed to model the flow phenomena at the mesoscopic scale, and the macroscopic flow properties, such as the flow density and momentum, can be determined via distribution functions in phase space. The resulting information then enables the fundamental quantities such as the drag or lift forces to be computed. Overall, the LBM with single-relaxation Bhatnagar–Gross–Krook (BGK) model provides a convenient and straightforward approach for solving continuum flow problems described by the Navier–Stokes equations at moderate Reynolds numbers of approximately $O(10^2)$. In recent years, the LBM has been improved to handle the flows at higher Reynolds numbers by using the appropriate turbulent LB models with the multi-relaxation time (MRT) model [5,6].

A major advantage of lattice Boltzmann method is the ease and accuracy with which it enables complicated boundary geometries to be processed, hence, investigating suitable boundary conditions for LB simulations has become a highly researched area in many engineering and scientific applications. The bounce-back (BB) scheme provides a particularly straightforward approach for modeling no-slip conditions on solid surfaces in macroscopic flows. In this scheme, the outgoing directions of the distribution function at the boundary sites are simply specified as the reverse of the incoming directions. In practice, two basic types of BB scheme exist, namely the "on-site" [7] scheme and the "mid-plane" [8] scheme. As implied by their names, the physical boundary lies exactly at the lattice node in the former scheme, but lies in between the solid and the fluid lattice nodes in the latter. It is well-known that the on-site BB scheme is simpler, but has only first-order accuracy, whereas the mid-plane BB scheme provides second-order accuracy in both space and time [9–11].

Curved boundary treatments have been suggested as a means of improving the accuracy of the stair-shaped approximation conventionally used in LB simulations when the uniform lattice is mapped in space. Several strategies have been proposed for dealing with complex geometry, curved boundaries in LBM. The first approach is to use a body-fitted (arbitrary) mesh and to execute the distribution functions throughout the entire computational domain [12–14]. The second strategy also applies an interpolation-based approach, but under a uniform Cartesian mesh, to track the position of boundary. Then, the on-site or off-site BB scheme is executed at the boundary surface depending on the location of the boundary relative to the lattice nodes [15–21]. The final one is based upon the utilization of the immersed boundary treatments [22,23]. Due to their characteristics of a superior numerical accuracy, an intuitive approach and an inherent reliability, the interpolation type models published in [15–21] are the most commonly employed technique for resolving curved boundary problems in LB simulations. However, a previous study [20] has indicated that the interpolation routines used in these schemes to solve the distribution functions near the curved boundary result in a loss of mass conservation, which reduces the accuracy of the computed momentum transfer at the boundary and therefore results in a net mass flux. Consequently, the aim of the present study is to develop an interpolation-free treatment for modeling curved boundaries in LB simulations. Having verified the performance of the proposed scheme in a series of simulations involving a stationary square block within channel flows of various Reynolds numbers, the curved boundary treatment is then extended to the case of moving curved boundary problems by adding a momentum term to the bounced distribution functions at the solid surface.

The remainder of this paper is organized as follows. Section 2 briefly reviews the principles of the lattice Boltzmann method incorporating the single-relaxation Bhatnagar–Gross–Krook (BGK) approximation. Section 3 discusses the various interpolation-based curved boundary models presented in [15–21], then a concept of the interpolation-free is presented to develop two novel interpolation-free models for curved boundary treatments. The models are then extended by inserting a momentum term into the bounced distribution functions at the solid surface in order to develop schemes capable of modeling the fluid–solid interaction in LB simulations involving moving and curved boundaries. Section 4 commences by performing a series of numerical simulations in which a stationary square block is positioned at various axial locations within a channel flow. The results obtained for the flow rate, global density, drag force and lift force by the proposed interpolation-free schemes are compared with those obtained from the Filippova and Hänel [15–18], Bouzidi et al.

[19,20] and Yu [21] models, respectively. The proposed schemes are then applied to model the flow phenomena inherent in channel flows involving moving square and cylindrical blocks, respectively. Meanwhile, a Couette flow past the fixed square/cylinder block with the moving top/bottom walls is simulated to test the Galilean effect of the proposed model. Finally, Section 5 presents some brief conclusions and provides an indication of the intended direction of future research.

## 2. Review of lattice Boltzmann method

The fundamental principle of the lattice Boltzmann model is the use of distribution functions ($f$) based on kinetic theory to model the flow filed at the mesoscopic scale. Here, the density distribution function ($f$) represents the probability of the particles at site $x$ at time $t$ moving with a velocity $c_i$ during the time interval $\Delta t$ along each lattice link (i.e. direction) $i$. The lattice Boltzmann equation (LBE) is an explicit time-marching finite-difference representation of the continuous Boltzmann equation in phase space and time. The LBE incorporating the single relaxation Bhatnagar–Gross–Krook (BGK) approximation has the form [24]:

$$f_i(x + c_i\Delta t, t + \Delta t) - f_i(x,t) = \omega[f_i^{\mathrm{eq}}(x,t) - f_i(x,t)], \tag{1}$$

where $\omega \equiv \Delta t/\tau$ denotes the relaxation factor with limits $0 < \omega < 2$, $c_s = c/\sqrt{3}$ is the speed of sound, and $c = \Delta x/\Delta t$. The kinematic viscosity $v$ is given by the relaxation factor:

$$v = (2/\omega - 1)\Delta x \cdot c/6. \tag{2}$$

The local equilibrium distribution is an analog version of the Maxwellian distribution function for incompressible flows, and is expressed as:

$$f_i^{\mathrm{eq}}(x,t) = w_i\rho\left[1 + \frac{c_{iA}\cdot u_A}{c_s^2} + \frac{u_A u_B}{2c_s^2}\left(\frac{c_{iA}c_{iB}}{c_s^2} - \delta_{AB}\right)\right]. \tag{3}$$

In these expressions, the flow properties are defined as:

$$\text{Flow density}: \quad \rho = \sum_i f_i, \tag{4a}$$

$$\text{Momentum}: \quad \rho u_A = \sum_{iA} f_i c_{iA}. \tag{4b}$$

In the equations above, sub-indices $A$ and $B$ denote the components of the Cartesian coordinates with implied summation for repeated indices. Furthermore, $w_i$ is the weighting which can be determined to achieve isotropy of the fourth-order tensor of velocities and Galilean invariance [24]. Applying the Chapman–Enskog expansion, the continuity equation and the Navier–Stokes equations can be recovered exactly at the second-order approximation from the LB Eq. (1) if the density variation is sufficiently small [25].

For the D2Q9 (two-dimensional nine-velocities) model, the weightings in Eq. (3) are assigned as follows: $w_i = 4/9$ for $|c_i| = 0$ (i.e. static particle), $w_i = 1/9$ for $|c_i| = 1$, and $w_i = 1/36$ for $|c_i| = \sqrt{2}$. The lattice Boltzmann method applies two essential steps, namely collision and propagation, to reveal the flow phenomena at the mesoscopic scale. Hence, the corresponding computations of LBM are performed as:

$$\text{Collision step}: \quad \tilde{f}_i(x,t) = f_i(x,t) + \omega[f_i^{\mathrm{eq}}(x,t) - f_i(x,t)], \tag{5a}$$

$$\text{Propagation step}: \quad f_i(x + c_i\Delta t, t + \Delta t) = \tilde{f}_i(x,t), \tag{5b}$$

where $\tilde{f}_i$ denotes the post-collision state of the distribution function. From Eqs. (5a) and (5b), it is clear that the collision process is fully local and the propagation of the distribution functions is uniform. As a result, the lattice BGK scheme is very simple when applied with the unity lattice size (i.e. $\Delta x = \Delta y = 1$), and a relative time-step of $\Delta t = 1$ such that $c = \Delta x/\Delta t = 1$.

## 3. Boundary treatments at solid curved surfaces

LB simulations generally apply one of the interpolation-based schemes when treating boundaries with complex geometries comprising arbitrary curvatures, namely the Filippova and Hänel (FH) model [15–18] or the

Bouzidi/Yu [19–21] model. In both cases, interpolation is performed only near the boundary nodes rather than throughout the entire computational domain based on the uniform mesh defined on Cartesian coordinate.

Fig. 1 presents a schematic illustration of a regular lattice in 1D projection, involving the 2D or 3D body, and a curved boundary surface ($\mathbf{r}_W$). In simulating the curved boundary problems, this boundary surface may be located off the solid node ($\mathbf{r}_S$) or off the middle between solid and fluid nodes ($\mathbf{r}_S$ and $\mathbf{r}_F$). As shown, the fraction of the link located in the fluid region can be expressed using a parameter $q$, defined as:

$$q \equiv \frac{|\mathbf{r}_F - \mathbf{r}_W|}{|\mathbf{r}_F - \mathbf{r}_S|} = \frac{|\mathbf{r}_F - \mathbf{r}_W|}{\Delta x} \quad \text{within range } 0 < q \leqslant 1 \tag{6}$$

In Fig. 1, suppose that the particle distribution function moves from $\mathbf{r}_F$ to $\mathbf{r}_S$ with velocity $c_i$, and then reverses from $\mathbf{r}_S$ to $\mathbf{r}_F$ with $c_{-i} = -c_i$ to simulate the resulting momentum transfer at the curved boundary surface, i.e. the inherent bounce-back (BB) scheme. Meanwhile, for a moving wall treatment using the BB scheme, a certain amount of momentum must be added to the bounced distribution function to reflect the fluid–solid interaction (i.e. the momentum transfer) at the boundary surfaces. In other words, the distribution function should be formulated in the form [2] as:

$$f_{-i}(\mathbf{r}_S) = f_i(\mathbf{r}_S) + 6w_i \frac{\rho}{c^2}(c_{-i} \cdot u_W), \tag{7}$$

where $\rho$ is the fluid density at the wall and the wall travel with a velocity $u_W$. However, for a curved boundary, the reversed distribution function $f_{-i}(\mathbf{r}_F, t + \Delta t)$, after propagation step, should be modified using one of the curved boundary treatments, since the bounce-back event at the boundary surface ($\mathbf{r}_W$) may not be positioned exactly at a solid node ($\mathbf{r}_S$) or at the mid-point positions between the solid and fluid nodes ($\mathbf{r}_S$ and $\mathbf{r}_F$), respectively, i.e. $q \neq 1$ or $q \neq \frac{1}{2}$.

The present investigation commences by examining three conventional interpolation-based models for curved boundary treatment. Two interpolation-free techniques designed to improve the computational accuracy of the LB simulation results for flow problems involving a stationary, curved boundary condition are then formulated. Finally, the proposed interpolation-free models are extended via the addition of a momentum term and applied to the solution of moving, curved boundary condition problems.

### 3.1. Filippova and Hänel (FH) model for curved boundary treatment

Filippova and Hänel [15] were the first two researchers to present a curved boundary treatment for lattice-BGK models. Their model (referred to hereinafter as the FH model) enabled curved solid walls to be treated with second order accuracy, but was somewhat unstable. In an attempt to improve the numerical stability of the FH model, Mei et al. proposed an improved curved boundary treatment [16] and demonstrated its use in the simulation of 3D flows involving curved geometries [17,18]. The basic principles of the FH model are described in the following.

As shown in Fig. 1, the value of $f_{-i}(\mathbf{r}_F, t + \Delta t)$ following propagation step, which is equal to $\tilde{f}_{-i}(\mathbf{r}_S, t)$ following collision but prior to propagation step at time-level $t$, should be solved according to the given information in the surrounding fluid nodes, e.g. $\tilde{f}_i(\mathbf{r}_F, t)$, $\tilde{f}_i(\mathbf{r}'_F, t)$, and $\tilde{f}_i(\mathbf{r}''_F, t)$, etc. In [16], Mei et al. provided

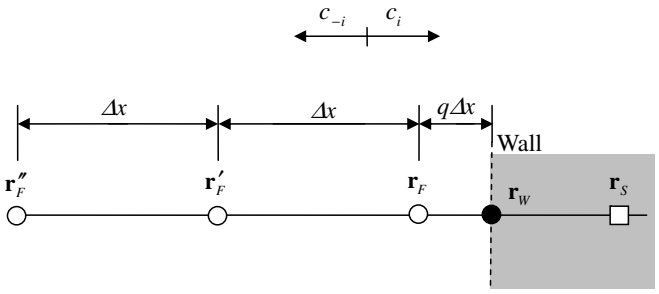


Fig. 1. 1D projection of regular lattice and curved boundary.

the detailed formulation and analysis of the FH model. Applying a process of linear interpolation, the unknown value of $\tilde{f}_{-i}(\mathbf{r}_S, t) = f_{-i}(\mathbf{r}_F, t + \Delta t)$ can be formulated as:

$$\tilde{f}_{-i}(\mathbf{r}_S, t) = (1 - \chi)\tilde{f}_i(\mathbf{r}_F, t) + \chi \cdot f_i^*(\mathbf{r}_S, t). \tag{8a}$$

In which the fictitious equilibrium distribution function $f_i^*$ has the form:

$$f_i^*(\mathbf{r}_S, t) = w_i \rho(\mathbf{r}_F)\left[1 + \frac{3}{c^2}(c_i \cdot u_{SF}) + \frac{9}{2}\frac{(c_i \cdot u_F)^2}{c^4} - \frac{3}{2}\frac{u_F^2}{c^2}\right], \tag{8b}$$

where $u_F \equiv u(\mathbf{r}_F, t)$, $\chi$ is a weighting factor, and $u_{SF}$ is the fictitious velocity which is to be chosen. Based on Filippova and Hänel's work, the FH model considered flows with a "slow-flow" condition, i.e. $\frac{L}{ct} \ll 1$, and the Taylor series expansion was applied in both space and time near the wall. The value of the weighting factor $\chi$ can be obtained once $u_{SF}$ is chosen. In [15], the relevant equations pertaining to FH model can be summarized as follows:

$$q < \frac{1}{2}: \quad u_{SF} = u_F, \quad \chi = \frac{\omega \cdot (2q - 1)}{(1 - \omega)}, \tag{9a}$$

$$q \geqslant \frac{1}{2}: \quad u_{SF} = \frac{(q - 1)}{q} \cdot u_F + \frac{1}{q} u_W, \quad \chi = \omega \cdot (2q - 1), \tag{9b}$$

where the velocity of the moving boundary $u_W$ is given.

The flexibility in the construction of the fictitious equilibrium distribution function $f_i^*(\mathbf{r}_S, t)$ is the key to achieving an improved numerical stability and computational accuracy. To improve the numerical stability, Mei et al. [16–18] suggested using different nodes to obtain $\tilde{f}_{-i}(\mathbf{r}_S, t)$. Accordingly, Eqs. (9a) and (9b) were modified to the following forms:

$$q < \frac{1}{2}: \quad u_{SF} = u_{FF}, \quad \chi = \frac{\omega \cdot (2q - 1)}{(1 - 2\omega)}, \tag{10a}$$

$$q \geqslant \frac{1}{2}: \quad u_{SF} = \left(1 - \frac{3}{2q}\right) \cdot u_F + \frac{3}{2q} u_W, \quad \chi = \frac{2\omega \cdot (2q - 1)}{(2 + \omega)}, \tag{10b}$$

where $u_{FF} \equiv u(\mathbf{r}'_F, t)$ in Eq. (10a), as shown in Fig. 1.

In applying the FH model to treat curved boundaries in the current LB simulations, Eqs. (10a) and (10b) are used to obtain the values of $u_{SF}$ and $\chi$, and these values are then substituted into Eq. (8b) to get $f_i^*(\mathbf{r}_S, t)$. Finally, $\tilde{f}_{-i}(\mathbf{r}_S, t)$ is solved from Eq. (8a).

### 3.2. Bouzidi and Yu interpolation-based models for curved boundary treatment

In LB simulations involving wall boundaries, both the momentum transfer experienced by the particles which encounter the boundary and the corresponding distribution functions are determined by the fluid–solid interaction. For a rigid wall with no-slip condition, the bounce-back (BB) boundary treatment is the most easily implemented scheme and is therefore widely used in LBM simulations. Accordingly, Bouzidi et al. in [19] proposed a method for treating curved boundaries by combining the BB scheme with an interpolation approach. In a later study, Lallemand and Luo [20] applied the same approach to treat moving boundary problems, hereinafter namely the Bouzidi's model.

In LBM, the particle velocity is always specified as unity, i.e. $c_i \equiv \Delta x/\Delta t = 1$. When the mid-plane BB scheme is applied in Bouzidi's curved boundary model, the interpolation of the distribution function $f_{-i}(\mathbf{r}_F, t + \Delta t)$ following the propagation step should be formulated based on different lattice nodes and time-levels according to which situations of the arbitrary location is in established [20], i.e. $q < \frac{1}{2}$ or $q \geqslant \frac{1}{2}$. When linear interpolation is applied, Bouzidi's model can be formulated as:

$$\tilde{f}_{-i}(\mathbf{r}_S, t) = 2q \cdot \tilde{f}_i(\mathbf{r}_F, t) + (1 - 2q)\tilde{f}_i(\mathbf{r}'_F, t) \quad \text{for } q < \frac{1}{2}, \tag{11a}$$

$$\tilde{f}_{-i}(\mathbf{r}_S, t) = \frac{1}{2q}\tilde{f}_i(\mathbf{r}_F, t) + \frac{(2q - 1)}{2q}\tilde{f}_{-i}(\mathbf{r}_F, t) \quad \text{for } q \geqslant \frac{1}{2}. \tag{11b}$$

Alternatively, when quadratic interpolation is applied, the model has the form:

$$\tilde{f}_{-i}(\mathbf{r}_S,t) = q(1+2q)\tilde{f}_i(\mathbf{r}_F,t) + (1-4q^2)\tilde{f}_i(\mathbf{r}'_F,t) - q(1-2q)\tilde{f}_i(\mathbf{r}''_F,t) \quad \text{for } q < \frac{1}{2}, \tag{11c}$$

$$\tilde{f}_{-i}(\mathbf{r}_S,t) = \frac{1}{q(2q+1)}[\tilde{f}_i(\mathbf{r}_F,t) - (1-4q^2)\tilde{f}_{-i}(\mathbf{r}_F,t) + q(1-2q)\tilde{f}_{-i}(\mathbf{r}'_F,t)] \quad \text{for } q \geqslant \frac{1}{2}. \tag{11d}$$

From the equations above, it is clear that Bouzidi's model with mid-plane BB scheme requires separate treatments for $q < \frac{1}{2}$ and $q \geqslant \frac{1}{2}$, respectively. This is not only inconvenient from a computer coding point of view, but may also cause an abrupt change in the distribution functions ($f$) when $q$ changes from less than 1/2 to greater than 1/2. Accordingly, a unified treatment for curved boundaries was proposed by Yu et al. [21] based on the same concept as that applied by Bouzidi et al. [19]. In the proposed approach (referred to hereafter as Yu's model), the on-site BB scheme was applied in place of the mid-plane BB scheme, thus avoiding the requirement to judge the positions based on the value of $q$ when interpolating the unknown distribution function. However, the model requires two sequences of interpolations at different time-levels. In Yu's model, the first interpolation sequence is applied to obtain the distribution function $f_{-i}(\mathbf{r}_W, t+\Delta t)$ following propagation, while the second interpolation is performed to obtain the value of $f_{-i}(\mathbf{r}_F, t+\Delta t)$ based on the interpolated value of $f_{-i}(\mathbf{r}_W, t+\Delta t)$. From a coding perspective, it is convenient to combine the propagation and bounce-back process into one single step. As a result, the value of $f_{-i}(\mathbf{r}_F, t+\Delta t) = \tilde{f}_{-i}(\mathbf{r}_S, t)$ can be formulated based on the conjunctive results obtained by the two interpolation sequences.

When linear interpolation is applied, Yu's model can be formulated as:

$$\tilde{f}_{-i}(\mathbf{r}_S,t) = \frac{1}{(1+q)}[q\cdot\tilde{f}_i(\mathbf{r}_F,t) + (1-q)\cdot\tilde{f}_i(\mathbf{r}'_F,t) + q\cdot\tilde{f}_{-i}(\mathbf{r}_F,t)]. \tag{12a}$$

Meanwhile, if quadratic interpolation is applied, the model has the form:

$$\begin{aligned}\tilde{f}_{-i}(\mathbf{r}_S,t) = \frac{1}{(2+q)(1+q)}&[q(1+q)\cdot\tilde{f}_i(\mathbf{r}_F,t) + 2(1-q^2)\cdot\tilde{f}_i(\mathbf{r}'_F,t) - q(1-q)\cdot\tilde{f}_i(\mathbf{r}''_F,t)\\ &+ 2q(2+q)\cdot\tilde{f}_{-i}(\mathbf{r}_F,t) - q(1+q)\cdot\tilde{f}_{-i}(\mathbf{r}'_F,t)].\end{aligned} \tag{12b}$$

Overall, the major features of these two interpolation-based models proposed by Bouzidi and Yu, respectively, can be summarized as follows:

(a) Yu's model provides a unified scheme for the treatment of curved boundaries and does not require the judgment of wall position by $q$ for computational purposes.
(b) Bouzidi's model requires only a single interpolation sequence at different time-level, with the formulation of the interpolation depending on the evaluated condition of $q$. However, Yu's model inevitably involves two interpolation sequences.
(c) For the case, where $q = 1/2$, Bouzidi's model recovers the mid-plane BB scheme using Eqs. (11b) and (11d). However, in Yu's model, the on-site BB scheme cannot be satisfied when $q = 1$, since the second interpolation sequence performed to obtain $f_{-i}(\mathbf{r}_F, t+\Delta t)$ is still required to model the curved boundary conditions when $q = 1$.
(d) In Bouzidi's model, the on-site BB scheme cannot be recovered when $q = 1$. In other words, only the mid-plane BB scheme is satisfied when $q = 1/2$, but the on-site BB scheme is not considered in Bouzidi's model.

A major difference between the FH model presented in Section 3.1 and the Bouzidi and Yu interpolation-based models presented in this section is that the former scheme (i.e. FH model) formulates a fictitious distribution function at the solid nodes and then executes the collision step at these nodes, whereas the latter models (i.e. Bouzidi and Yu models) solve the unknown values of $f_{-i}(\mathbf{r}_F, t+\Delta t)$ at the fluid nodes using an interpolation technique without the collision step.

### 3.3. An interpolation-free model for curved boundary treatment

According to the previous investigation by Lallemand and Luo [20], interpolation-based schemes for treatment of curved boundaries destroy mass conservation near the boundary. The resulting errors in the computed results for the momentum transfer at the boundary leads to a net mass flux. Therefore, this study proposes two interpolation-free approaches for curved boundary treatment in LB simulations in order to improve the accuracy of the computed results.

The proposed approaches are based upon the following principles:

(a) Both mass and momentum conservation should be satisfied, i.e. $\rho = \sum_{i=0}^{b} f_i^{\mathrm{eq}}$ and $\rho u = \sum_{i=1}^{b} c_i f_i^{\mathrm{eq}}$. In other words, the values of the equilibrium distribution functions ($f_i^{\mathrm{eq}}$) near the boundary cannot be changed by the proposed curved boundary model.
(b) If this curved boundary model in LBM maintains the two essential steps, i.e. the collision and propagation steps, with the same time interval (i.e. $\Delta t = 1$), the kinematic viscosity must be equal for the smaller lattice size near the curved boundary, e.g. $q \leqslant 1$.
(c) Since the principle of $f_i(x,t) = f_i^{\mathrm{eq}}(x,t) + f_i^{\mathrm{neq}}(x,t)$ is hold in LBM, where $f_i^{\mathrm{neq}}$ is the non-equilibrium part of the distribution function, based on which the deviatoric stresses are evaluated. Furthermore, the deviatoric stresses between different lattice sizes must be continuous, and thus $(1-\frac{\omega}{2})f_i^{\mathrm{neq}}$ should be equal in the different lattice sizes by applying the following definition of the deviatoric (non-equilibrium part) stresses: $\tau_{AB} = (1-\frac{\omega}{2})\sum_{i=1}^{b} f_i^{\mathrm{neq}} \times (c_{iA}c_{iB} - \frac{1}{2}c_i \cdot c_i \delta_{AB})$.

Applying the principles described above, the proposed interpolation-free approaches treat curved boundaries using an appropriate local refinement grid technique with a BB scheme at the solid surface. As shown in Fig. 2, for an instance of the proposed interpolation-free model, the distribution functions directed toward the curved boundary, i.e. $f_3$, $f_4$, and $f_7$, are treated as the values from "coarse" grid transferring into the "fine" grid in accordance with the value of $q \cdot \Delta x$ at each link using a 1D grid refinement technique, and a BB scheme is then applied at the surface of the curved solid. Filippova and Hänel [15] proposed a grid refinement technique which not only satisfies the principles outlined above, but also requires no interpolation. Therefore, Filippova and Hänel's grid refinement technique provides a suitable basis for the interpolation-free curved boundary treatments proposed in the current study. Note that the Filippova and Hänel's grid refinement technique was not applied to handle the curved boundary problems in literature [15] and the stair-shaped grid approximation was still maintained for the solid boundary nodes. The FH's curved boundary model presented in Section 3.1 has no relevance to the Filippova and Hänel's grid refinement approach. The details of the proposed methods are described in the following paragraphs.

When transferring information between nodes associated with different lattice sizes, it is essential to rescale the distribution functions at each link ($f_i$) in order to satisfy the principles of mass and momentum

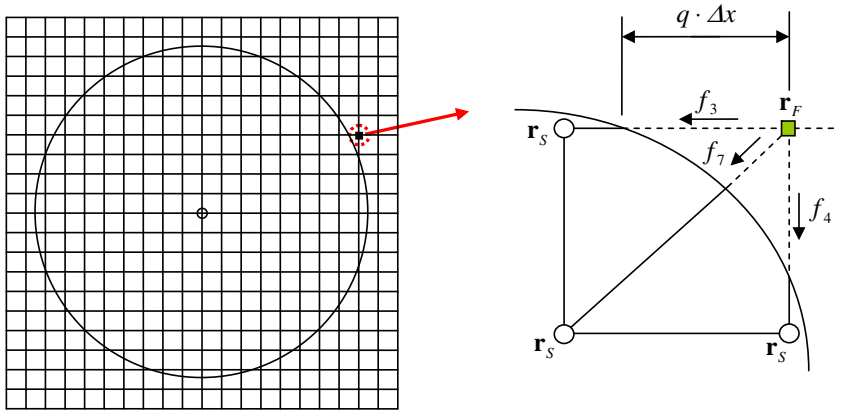


Fig. 2. Illustration of interpolation-free treatment of curved boundary using local refinement concept.

conservation, respectively, and to ensure a continuity of the deviatoric stresses across the interface between the two different grids. In the LBM framework, the kinematic viscosity is defined as $v = (2/\omega - 1)\Delta x \cdot c/6$ for a given lattice size $\Delta x$. In rescaling the distribution functions, the following grid size ratio is defined: $Q' \equiv \frac{\Delta x^{(f)}}{\Delta x^{(c)}}$, where superscripts (c) and (f) denote the coarse grid and the fine grid quantities, respectively. To ensure a consistent viscosity and Reynolds number in the coarse lattice ($\Delta x^{(c)}$) and fine lattice ($\Delta x^{(f)}$), the relationship between the two relaxation factors of the two different lattices must conform to:

$$\omega^{(f)} = \frac{2Q'}{Q' + \left(\frac{2}{\omega^{(c)}} - 1\right)}. \tag{13}$$

The relaxation factor ($\omega$) is changed with the grid size and the hydrodynamic variables (e.g. the kinematic viscosity). Furthermore, the derivatives of the distribution functions must be continuous across the interface between the two different grids. Consequently, the following relationship is applied between the post-collision distribution functions ($\tilde{f}_i$) at adjacent nodes in the coarse and fine lattices:

$$\tilde{f}_i^{(f)} = f_i^{eq(c)} + (\tilde{f}_i^{(c)} - f_i^{eq(c)}) \cdot \frac{Q'\omega^{(c)}(1-\omega^{(f)})}{\omega^{(f)}(1-\omega^{(c)})}. \tag{14}$$

In the proposed model, Eqs. (13) and (14) are applied in place of interpolation to treat the curved boundary.

In present study, the FH's transformation [15] described above is integrated with the on-site BB scheme to construct the so-called OSIF (on-site interpolation-free) model. In the proposed model, the fluid distribution function $\tilde{f}_i(\mathbf{r}_F, t)$, is already computed in the post-collision step and is then streamed to the surface of the solid node $\mathbf{r}_W$ in the propagation step, i.e. the $f_i(\mathbf{r}_W, t + \Delta t)$. The on-site BB scheme is then applied at the solid surface, i.e. by setting $\tilde{f}_{-i}(\mathbf{r}_W, t + \Delta t) = f_i(\mathbf{r}_W, t + \Delta t)$ in the following collision step. Finally, the distribution function is streamed back to the fluid node in the subsequent propagation step to obtain $f_{-i}(\mathbf{r}_F, t + 2\Delta\ t)$ at time-level $(t + 2\Delta t)$. When applying the on-site BB scheme, it is only necessary to transform the distribution function from the coarse grid to the fine grid because parameter $q$ is always less than or equal to 1. Therefore, the OSIF model can be formulated as a unified form as:

For $0 < q \leqslant 1$: $Q' \equiv \frac{\Delta x^{(f)}}{\Delta x^{(c)}} = q$, and $\omega^{(c)} = \omega$ is given, and thus

$$\omega^{(f)} = \frac{2Q'}{Q' + (\frac{2}{\omega^{(c)}} - 1)} \quad \text{and}$$

$$\tilde{f}_i(\mathbf{r}_F, t) = f_i^{eq}(\mathbf{r}_F, t) + [\tilde{f}_i(\mathbf{r}_F, t) - f_i^{eq}(\mathbf{r}_F, t)] \cdot \frac{Q'\omega^{(c)}(1-\omega^{(f)})}{\omega^{(f)}(1-\omega^{(c)})}. \tag{15}$$

In the OSIF model, the term $\tilde{f}_i(\mathbf{r}_F, t)$ in left-hand side of Eq. (15) is revised by the transformation $\tilde{f}_i^{(c)}(\mathbf{r}_F, t) \to \tilde{f}_i^{(f)}(\mathbf{r}_F, t)$ at the same lattice site $\mathbf{r}_F$ and the same time-level $t$. Afterwards, the computed $\tilde{f}_i(\mathbf{r}_F, t)$ is streamed to the boundary node $\mathbf{r}_W$ in the following propagation step (i.e. $f_i(\mathbf{r}_W, t + \Delta t) = \tilde{f}_i(\mathbf{r}_F, t)$), and then apply the on-site bounce-back scheme: $\tilde{f}_{-i}(\mathbf{r}_W, t + \Delta t) = f_i(\mathbf{r}_W, t + \Delta t)$ in the collision step. Finally, the $f_{-i}(\mathbf{r}_F, t + 2\Delta t) = \tilde{f}_{-i}(\mathbf{r}_W, t + \Delta t)$ is subsequently streamed back to the fluid node $\mathbf{r}_F$ from the boundary $\mathbf{r}_W$ at time-level $(t + 2\Delta t)$. From the coding perspective, the on-site BB scheme is directly applied at the solid node $\mathbf{r}_S$ for convenient, i.e. setting $\tilde{f}_i(\mathbf{r}_F, t) = f_i(\mathbf{r}_W, t + \Delta t) = f_i(\mathbf{r}_S, t + \Delta t)$ at solid node in propagation step and $\tilde{f}_{-i}(\mathbf{r}_W, t + \Delta t) = \tilde{f}_{-i}(\mathbf{r}_S, t + \Delta t)$ in following bounce-back (collision) step. Furthermore, it is clearly observed that the on-site BB scheme can be recovered when $Q' = q = 1$ with conditions of $\omega = \omega^{(f)} = \omega^{(c)}$ and $\tilde{f}_i^{(f)}(\mathbf{r}_F, t) = \tilde{f}_i^{(c)}(\mathbf{r}_F, t)$.

To reduce the deviation in the non-equilibrium parts of distribution function caused by the transfer procedure, this study proposes a second interpolation-free model with a "composite" bounce-back scheme, designated as the CPIF (composite interpolation-free) model which applies either the on-site BB scheme or the mid-plane BB scheme depending on the evaluated conditions of $q$. Specifically, when $q \leqslant 1/2$, the mid-plane BB scheme is applied, whereas if $q$ lies in the range $1/2 < q \leqslant 1$, the on-site BB scheme is employed. In other words, the CPIF model can be formulated as:

$$\omega^{(c)} = \omega \quad \text{is given,} \quad \text{so } \omega^{(f)} = \frac{2Q'}{Q' + (\frac{2}{\omega^{(c)}} - 1)}.$$

For $q \leqslant \frac{1}{2}$: applying the mid-plane BB scheme, so that $Q^{'} = 2q$ and

$$\tilde{f}_{-i}(\mathbf{r}_S, t) = f_i^{eq}(\mathbf{r}_F, t) + [\tilde{f}_i(\mathbf{r}_F, t) - f_i^{eq}(\mathbf{r}_F, t)] \cdot \frac{Q'\omega^{(c)}(1-\omega^{(f)})}{\omega^{(f)}(1-\omega^{(c)})}. \tag{16a}$$

For $q > \frac{1}{2}$: applying the on-site BB scheme, so that $Q^{'} = q$ and

$$\tilde{f}_i(\mathbf{r}_F, t) = f_i^{eq}(\mathbf{r}_F, t) + [\tilde{f}_i(\mathbf{r}_F, t) - f_i^{eq}(\mathbf{r}_F, t)] \cdot \frac{Q'\omega^{(c)}(1-\omega^{(f)})}{\omega^{(f)}(1-\omega^{(c)})}. \tag{16b}$$

It is clear that the CPIF model is not a unified model. However, a benefit of computation is appeared, such that both the mid-plane and on-site BB schemes can be recovered when $q = 1/2$ and $q = 1$, respectively, i.e. $\tilde{f}_{-i}(\mathbf{r}_S, t) = \tilde{f}_i(\mathbf{r}_F, t)$ when $q = 1/2$, $\tilde{f}_i^{(f)}(\mathbf{r}_F, t) = \tilde{f}_i^{(c)}(\mathbf{r}_F, t)$ when $q = 1$, with conditions of $\omega = \omega^{(f)} = \omega^{(c)}$ both for $q = 1/2$ and $q = 1$. Meanwhile, it should be noted that the on-site BB treatment is applied at solid node $\mathbf{r}_S$ when Eq. (16b) is used for $q > 1/2$, i.e. setting $\tilde{f}_{-i}(\mathbf{r}_S, t + \Delta t) = f_i(\mathbf{r}_F, t)$ at solid nodes in following bounce-back (collision) step.

When the transformation $\omega^{(c)} \to \omega^{(f)}$ is applied to ensure the consistent kinematic viscosity in the coarse grid and the fine grid near the boundary surface. The condition of $\omega^{(f)} \leqslant \omega^{(c)}$ is always established and their values depend on the grid size ratio, $Q^{'} \equiv \Delta x^{(f)}/\Delta x^{(c)}$. It is clear that larger difference between the values of $\omega^{(f)}$ and $\omega^{(c)}$ can be obtained when the $Q^{'}$ value is small. Under such condition, the computational instability may be caused. However, both $\omega^{(f)}$ and $\omega^{(c)}$ should satisfy the limits $0 < \omega < 2$ in LB simulations, such that the coarse grid relaxation factor $\omega^{(c)}$ must be chosen carefully. Furthermore, according to the results reported in previous studies [2,18,26,27], the over-relaxation factor, i.e. $\omega > 1$, provides more accurate and stable results when using the single-relaxation LBGK model. Based on the reasons and the numerical tests in current work, the over-relaxation factor with limit $1.5 \geqslant \omega^{(c)} > 2$ is recommended both for the OSIF and CPIF models.

### 3.4. Application of curved boundary treatment to moving boundary problems

To extend the treatments for stationary curved boundaries described in the sections above to the case of moving boundary problems, it is necessary to add the momentum effect arising from the fluid–solid interaction at the moving boundary to the bounced distribution function at the solid node ($\mathbf{r}_S$). As indicated in Eq. (7), the momentum effect is given by $6w_i \frac{\rho}{c^2}(c_{-i} \cdot u_W)$.

Furthermore, applying an appropriate treatment of the nodes moving out of the non-fluid (solid) region into the fluid region is also important. However, this treatment to compute the unknown distribution functions is not unique. For example, the equilibrium distribution function at $\mathbf{r}_F$ can be computed by taking the moving boundary velocity ($u_W$) and the global average density in the system $\rho_0$ or local average density, and then applying the equilibrium distribution functions to obtain the unknown distribution functions. Alternatively, the distribution functions in the non-fluid region can be systematically updated by performing collisions as in the fluid region while maintaining the velocity at the same rate as that of the solid object, i.e. $u_W$. According to Lallemand and Luo [20], both approaches yield similar results.

In the present study, an extrapolation method is utilized to compute the unknown distribution functions. An assumption is made that the gradients of the distribution functions (i.e. $\frac{\partial f}{\partial x}$) of the nodes exiting the non-fluid region and entering the fluid region are equal to those of the distribution functions near the boundary. Accordingly, the gradients of the unknown distribution functions can be formulated by the second-order backward difference scheme as follows:

$$\left.\frac{\partial f}{\partial x}\right|_{\text{Boundary}} = \frac{3f_{-i}(\mathbf{r}_F, t) - 4f_{-i}(\mathbf{r}'_F, t) + f_{-i}(\mathbf{r}''_F, t)}{2\Delta x}, \tag{17a}$$

where $f_{-i}(\mathbf{r}_F, t)$ is the unknown value of the distribution functions of the node $\mathbf{r}_F$ leaving the non-fluid region and entering the fluid region. Meanwhile, the gradients of the distribution functions near the boundary are given by the second-order backward difference scheme as

$$\left.\frac{\partial f}{\partial x}\right|_{\text{near Boundary}} = \frac{3f_{-i}(\mathbf{r}'_F, t) - 4f_{-i}(\mathbf{r}''_F, t) + f_{-i}(\mathbf{r}''_F + c_{-i}\Delta t, t)}{2\Delta x}. \tag{17b}$$

Setting $\frac{\partial f}{\partial x}\big|_{\text{Boundary}} = \frac{\partial f}{\partial x}\big|_{\text{near Boundary}}$ gives

$$f_{-i}(\mathbf{r}_F, t) = \frac{7}{3} f_{-i}(\mathbf{r}'_F, t) - \frac{5}{3} f_{-i}(\mathbf{r}''_F, t) + \frac{1}{3} f_{-i}(\mathbf{r}''_F + c_{-i}\Delta t, t). \tag{18}$$

Eq. (18) provides an approach for evaluating the unknown distribution functions of the nodes entering the fluid region of the computational domain from the solid region. By applying the 'momentum exchange method' [8], the drag and lift forces imposed by the fluid on the solid body can then be evaluated via the formulation:

$$F_A = \sum_{\text{ALL } \mathbf{r}_S} \sum_{iA} c_{iA}[f_{iA}(\mathbf{r}_S, t) + f_{-iA}(\mathbf{r}_F, t)], \tag{19}$$

which is essentially a summary of the momentum flux over all the boundary located between lattice nodes $\mathbf{r}_S$ and $\mathbf{r}_F$, and orientated normal to $c_i$. An alternative method to estimate the drag and lift forces is the 'stress integration method' [14]. Based on the numerical results in previous studies, both methods for force evaluation can provide accurate results as long as the characteristic length of boundary is large enough in LB simulations, e.g. the $r > 8$ lattices across the cylinder radius for problem of flow past a stationary cylinder [2,18], and $x > 15$ lattices for an inclined boundary [28], etc. However, the 'momentum exchange method' is easy to implement and provides a superior results to estimate the drag force for problem of flow past a solid obstacle within range of $10 < Re < 100$. Consequently, the 'momentum exchange method' is applied for lift/drag forces evaluation in current work.

## 4. Simulations

In this study, the validity of the proposed OSIF and CPIF models is verified by performing a series of simulations in which a stationary square block is positioned at various locations along the length ($x$-locations) of a fluid-carrying channel. The results obtained using the present models are then compared with those obtained from the FH [15–18], Bouzidi [19,20] and Yu [21] models, respectively. Having demonstrated the feasibility of the proposed models, the CPIF model is then extended to the solution of moving, curved boundary problems in which a square block and a circular cylinder, respectively, move progressively along the longitudinal axis of a channel containing a stationary flow. In addition, to test the Galilean invariance of the proposed CPIF model, a Couette flow past the fixed square/cylinder block with the moving top/bottom walls is simulated.

### 4.1. Verification of curved boundary models using stationary square block

As shown in Fig. 3, the verification simulations consider a channel flow with a stationary square block positioned at various locations along the $x$-axis of the channel. The computational domain is mapped using a $500 \times 100$ mesh, and the stationary block is assumed to have a side-length of 24. During the simulations, the central position of the block is shifted from $Cx = 200$ to 201 in increments of 0.25, while maintaining a constant height of $Cy = 50$. Periodic boundary conditions are applied at the channel inlet and outlet for convenience. The simulations are performed at three different values of the channel Reynolds number, i.e. $Re = 90$, 165 and 325, respectively, where the channel Reynolds number is defined as $Re = \frac{U_m H}{\nu}$, in which

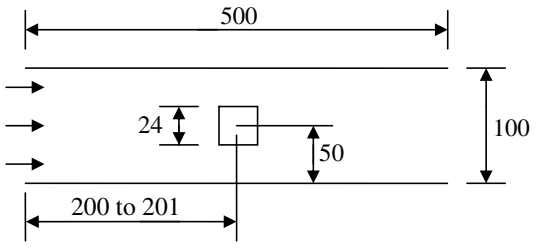


Fig. 3. Configuration of 2D channel flow with stationary square block with center located between $Cx = 200$ and 201.

$U_m$ is the average $x$-component velocity (i.e. $Ux$) at the channel outlet (i.e. $x = 500$) and $H$ is the height of the channel. In every case, the simulations are continued until the flow attains a steady state or a stable unsteady state (e.g. periodic vortex shedding). The simulations are also repeated using the pure mid-plane and on-site BB schemes in order to quantify the computational accuracies of the various schemes.

The performance of the various curved boundary treatment schemes is evaluated by comparing the results obtained from each method for the dimensionless flow rate ($Q^*$), the change in global density ($\rho'$), the dimensionless drag force ($Fx^*$), and the dimensionless lift force ($Fy^*$), respectively. The channel flow rate is evaluated as $Q = \int_0^H (U_x)\,dy$ at the channel outlet (i.e. $x = 500$). In the present study, a dimensionless flow rate is defined as $Q^* \equiv Q_{\text{Model}}/Q_{\text{MPBB}}$, where $Q_{\text{Model}}$ is the channel flow rate computed by the particular curved boundary model and $Q_{\text{MPBB}}$ is the channel flow rate obtained using the second-order accurate mid-plane BB scheme. Meanwhile, the change in global density ($\rho'$) is defined as the change in the global density throughout the domain from the initial condition (i.e. at time-step = 0) to the final steady state condition, i.e. $\rho' = \frac{|\rho_{\text{Initial}} - \rho_{\text{Steady}}|}{\rho_{\text{Initial}}} \times 100\%$. Finally, the drag force ($Fx$) and lift force ($Fy$) acting on the block are calculated from Eq. (19), and are both expressed in dimensionless form, i.e. $Fx^* \equiv (Fx)_{\text{Model}}/(Fx)_{\text{MPBB}}$ and $Fy^* \equiv (Fy)_{\text{Model}}/(Fy)_{\text{MPBB}}$, respectively. In presenting the results, all four performance evaluation metrics are truncated at values of less than $10^{-3}$ in order to eliminate the data noise caused by rounding errors during the computation process.

Fig. 4(a1–a3) and (b1–b3) presents the results obtained by the various curved boundary treatment methods for the variation in the dimensionless flow rate ($Q^*$) and the global density change rate ($\rho'$), respectively, with the varying positions of the block center from $Cx = 200$ to 201 at Reynolds numbers of $Re = 90$, 165, and 325, respectively. It is clear that there is no significant difference of the dimensionless flow rate ($Q^*$) computed by the mid-plane BB scheme and by the on-site BB scheme, in which the difference of $Q^*$ is less than 1.5%. Note that either the mid-plane or the on-site BB scheme has no change in global density, i.e. $\rho'_{\text{MPBB}} = \rho'_{\text{OSBB}} = 0$ as shown in Fig. 4(b1–b3). In general, the results show that steady state solutions are obtained at $Re = 90$ and 165, respectively. However, at a higher Reynolds number of $Re = 325$, the flow transits to unsteady state with periodic vortex shedding behind the stationary block.

Observing the results obtained using the Yu's and Bouzidi's interpolation-based models, it can be seen that: (a) the use of a quadratic interpolation scheme yields no significant improvement in the computational accuracy compared to that obtained using linear interpolation; (b) there is no appreciable difference in the numerical results obtained using these two models; (c) for $q = 1$ or $q = 0.5$, the interpolation process inevitably induces computational errors, i.e. neither the on-site BB scheme nor the mid-plane BB scheme is recovered; and (d) the error in the flow rate increases as $q$ deviates further from $q = 1$ and at higher values of the Reynolds number. In general, Fig. 4(a1–a3) shows that the flow rate results computed using the FH model are similar to those obtained from Yu's and Bouzidi's linear interpolation models. Observing the results obtained for the global density change rate in Fig. 4(b1–b3), it can be seen that an incorrect mass flux is produced when the FH, Yu and Bouzidi curved boundary treatment schemes are applied. However, it is apparent that the incorrect mass flux is significantly reduced when the proposed OSIF and CPIF models are employed. Furthermore, it can be seen that both interpolation-free models enable the on-site and mid-plane BB schemes to be recovered exactly when $q = 1$ or 1/2, respectively. In general, Fig. 4(a1–a3) and (b1–b3) indicates that both the flow rate error and the global density change rate ($\rho'$) error increase at higher values of the Reynolds number when the FH, Bouzidi and Yu models are employed to treat the curved boundary. However, the errors produced by the proposed OSIF and CPIF models are significantly less than those generated by these three interpolation-based schemes. The numerical accuracy of the various curved boundary treatments is compared in Fig. 5, which shows the $x$-direction velocity component ($Ux$) profile along the centerline of the channel at $Re = 165$ for the case in which the center of the block is located at $Cx = 200.25$. Note that the results computed by the mid-plane BB scheme at $Cx = 200.50$ and the on-site BB scheme at $Cx = 200$ are nearly identical. It is observed that the results obtained using the OSIF and CPIF models, respectively, are very similar. Furthermore, the incorrect mass flux are also observed at the positions in front of the block as shown in Fig. 5(b), near the block in Fig. 5(d), and near the channel outlet in Fig. 5(c) when the interpolation-based models, i.e. the FH and Bouzidi's linear interpolation models, are applied. The generated incorrect mass flux may induce the inaccurate fluid–solid momentum interaction when these interpolation-based models are used.

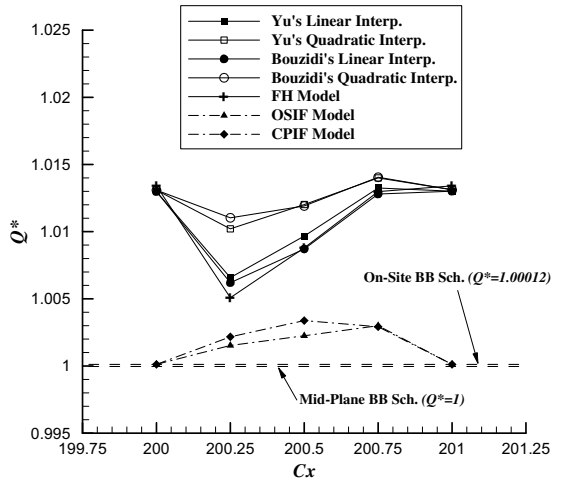


(a1)

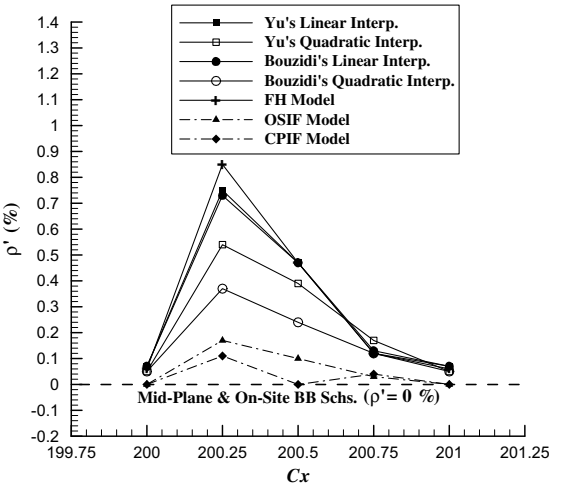


(b1)

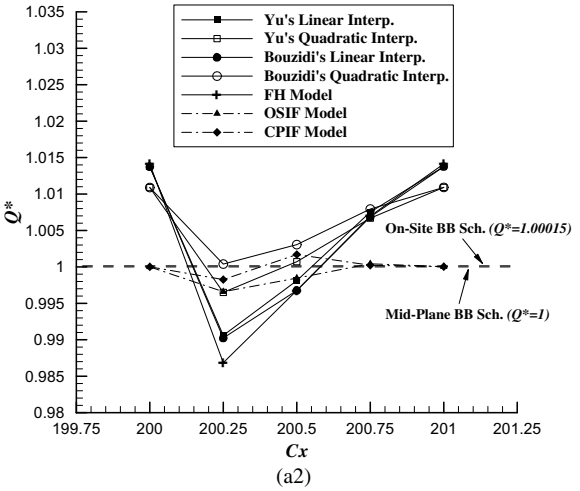


(a2)

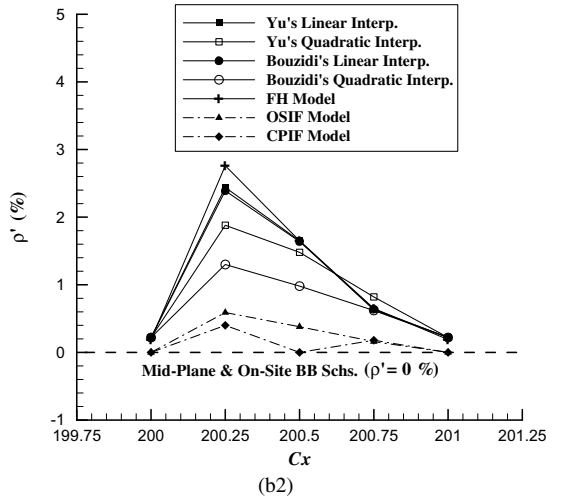


(b2)

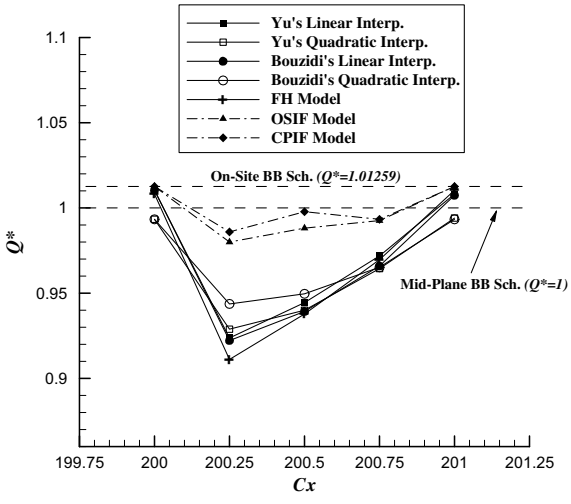


(a3)

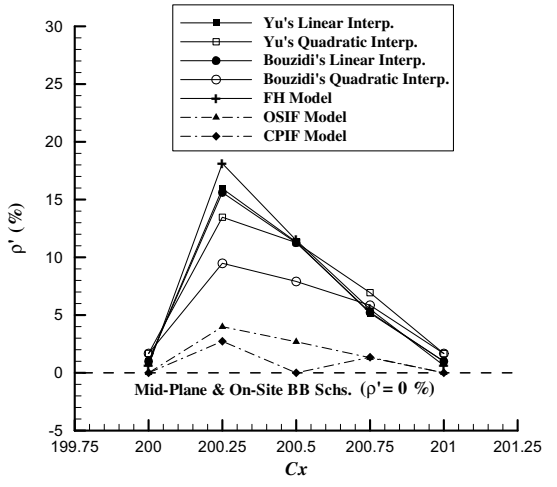


(b3)

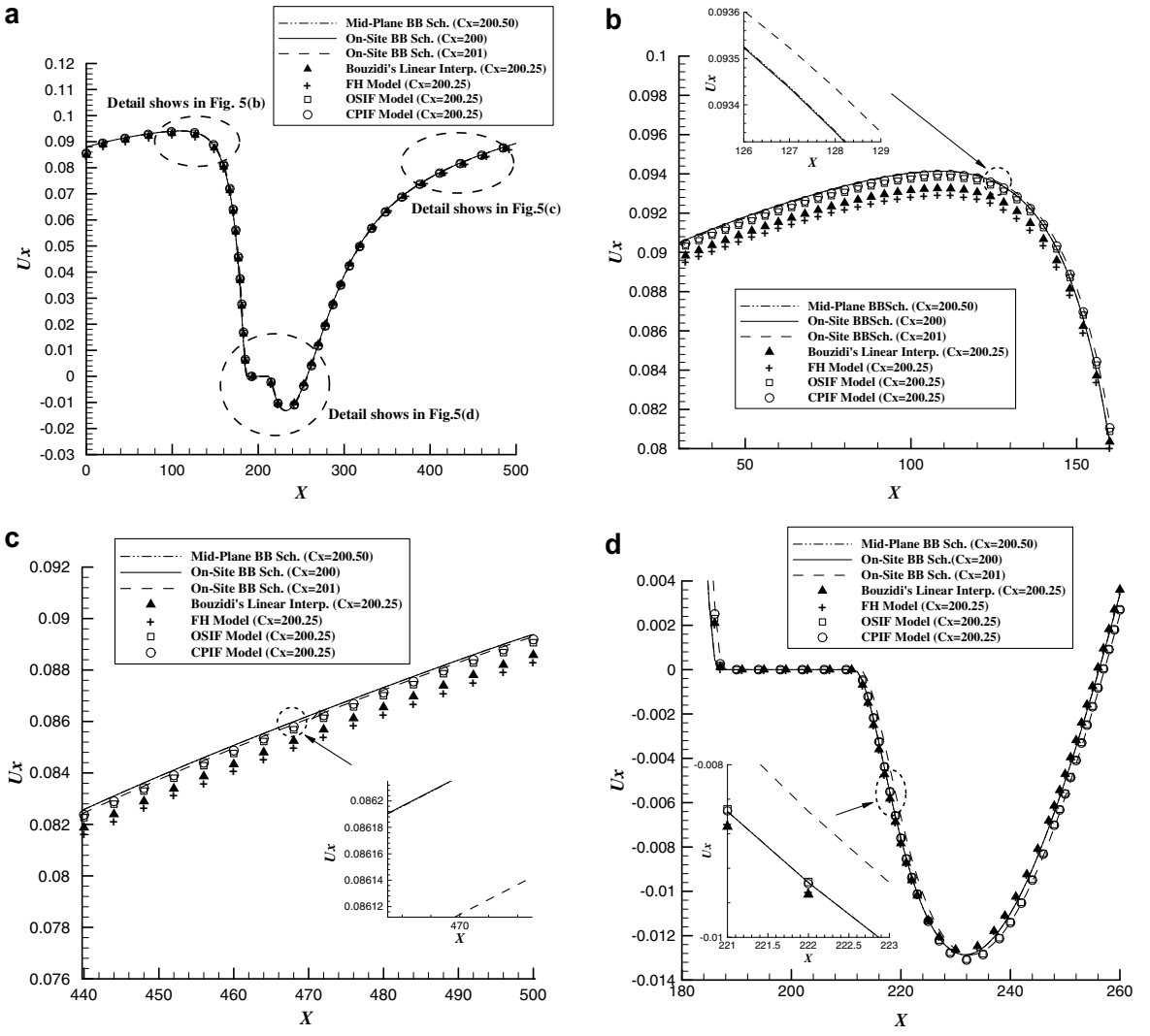


Fig. 5. $x$-Component velocity ($Ux$) profile along centerline of channel ($Cy = 50$) and $Cx = 200.25$ for channel Reynolds number of $Re = 165$: (a) $Ux$ profile along centerline of channel; (b) $Ux$ profile in front of block; (c) $Ux$ profile near channel outlet; (d) $Ux$ profile near square block.

Fig. 6(a1–a3) illustrates the variation of the dimensionless drag force ($Fx^*$) with the block center position for channel flows with Reynolds numbers of 90, 165 and 325, respectively. Fig. 6(b1–b2) presents the variation of the lift force ($Fy$) with computing time-steps at a Reynolds number of $Re = 325$. Note that equivalent results are not presented for $Re = 90$ and 165, respectively, since the corresponding lift force is found to be $Fy = 0$. In general, Fig. 6(a1–a3) shows that the results computed by the three interpolation-based schemes, i.e. the FH model, Yu's and the Bouzidi's models, for the drag force are broadly similar, and deviate by

Fig. 4. Numerical results obtained by different curved boundary treatments for channel flow with stationary square block: (a1) variation of dimensionless flow rate ($Q^*$) with block center location for channel Reynolds number of $Re = 90$ (time-steps = 25,000); (a2) variation of dimensionless flow rate ($Q^*$) with block center location for channel Reynolds number of $Re = 165$ (time-steps = 30,000); (a3) variation of dimensionless flow rate ($Q^*$) with block center location for channel Reynolds number of $Re = 325$ (time-steps = 60,000); (b1) variation of global density change rate ($\rho'$) with block center location for channel Reynolds number of $Re = 90$ (time-steps = 25,000); (b2) variation of global density change rate ($\rho'$) with block center location for channel Reynolds number of $Re = 165$ (time-steps = 30,000); (b3) variation of global density change rate ($\rho'$) with block center location for channel Reynolds number of $Re = 325$ (time-steps = 60,000).

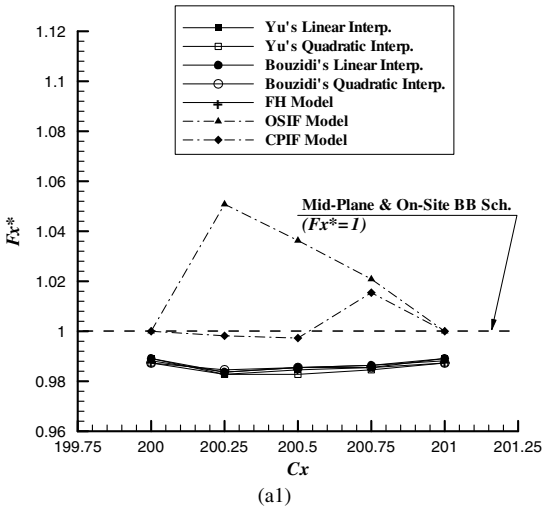
Yu's Linear Interp.
Yu's Quadratic Interp.
Bouzidi's Linear Interp.
Bouzidi's Quadratic Interp.
FH Model
OSIF Model
CPIF Model
Mid-Plane & On-Site BB Sch.
(Fx*=1)
Fx*
Cx

(a1)

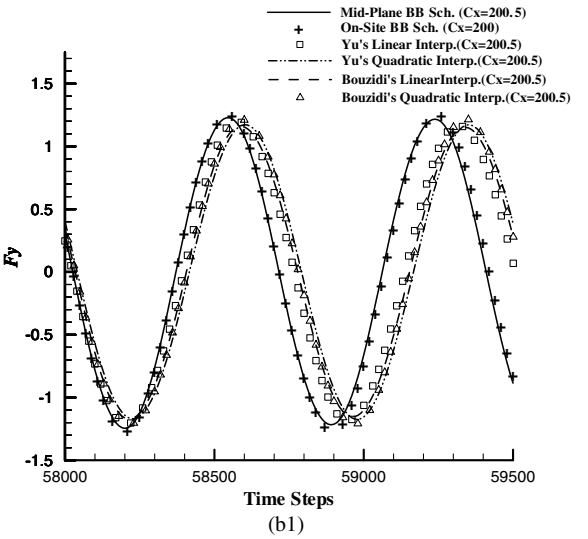
Mid-Plane BB Sch. (Cx=200.5)
On-Site BB Sch. (Cx=200)
Yu's Linear Interp.(Cx=200.5)
Yu's Quadratic Interp.(Cx=200.5)
Bouzidi's LinearInterp.(Cx=200.5)
Bouzidi's Quadratic Interp.(Cx=200.5)
Fy
Time Steps

(b1)

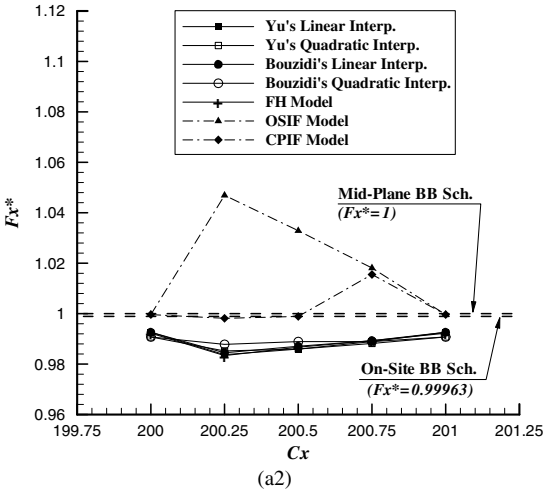
Yu's Linear Interp.
Yu's Quadratic Interp.
Bouzidi's Linear Interp.
Bouzidi's Quadratic Interp.
FH Model
OSIF Model
CPIF Model
Mid-Plane BB Sch.
(Fx*=1)
On-Site BB Sch.
(Fx*=0.99963)
Fx*
Cx

(a2)

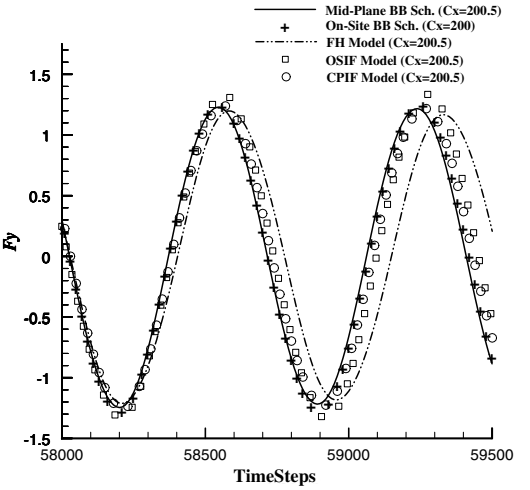
Mid-Plane BB Sch. (Cx=200.5)
On-Site BB Sch. (Cx=200)
FH Model (Cx=200.5)
OSIF Model (Cx=200.5)
CPIF Model (Cx=200.5)
Fy
TimeSteps

(b2)

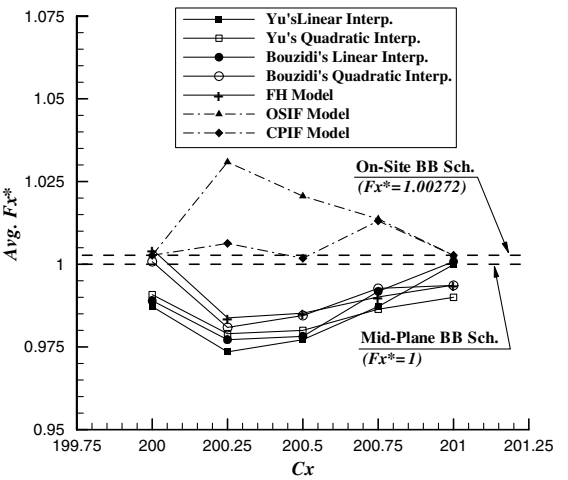
Yu'sLinear Interp.
Yu's Quadratic Interp.
Bouzidi's Linear Interp.
Bouzidi's Quadratic Interp.
FH Model
OSIF Model
CPIF Model
On-Site BB Sch.
(Fx*=1.00272)
Mid-Plane BB Sch.
(Fx*=1)
Avg. Fx*
Cx

(a3)

Table 1
Reliability analysis of OSIF/CPIF models for Reynolds number of $Re = 165$ and block center locations of $Cx = 200$, 200.5, and 201, respectively

| Curved boundary model | $Q^*$ | $\rho'$ (%) | $Fx^*$ | $Fy^*$ |
|---|---|---|---|---|
| OSIF model ($Cx = 200.01$) | 0.9949 | 0.78 | 1.0598 | 0 |
| OSIF model ($Cx = 200.99$) | 1.0024 | 0.06 | 1.0033 | 0 |
| CPIF model ($Cx = 200.01$) | 0.9949 | 0.77 | 0.9963 | 0 |
| CPIF model ($Cx = 200.49$) | 1.0019 | 0.02 | 1.0004 | 0 |
| CPIF model ($Cx = 200.51$) | 0.9982 | 0.40 | 1.0307 | 0 |
| CPIF model ($Cx = 200.99$) | 1.0024 | 0.06 | 0.9996 | 0 |

no more than 3% from the values computed using the mid-plane BB scheme. However, as exhibited in Fig. 6(b1–b2), the significant phases difference for the lift force ($Fy$) against the computing time-steps are observed when using the three interpolation-based models (FH, Bouzidi's, and Yu's models) due to the incorrect mass flux generated near the curved boundary. In addition, it is apparent that the OSIF model fails to improve the accuracy of the computed results for the drag and lift forces. However, the CPIF model substantially improves the accuracy of the mass flux calculation at the fluid–solid boundary, and therefore enhances the precision of the computed momentum interaction. Interestingly, mass flux errors are still generated in the current simulations even though the square block is stationary in the channel because the number of solid nodes dose not maintain constant as the center of the block is shifted incrementally from $Cx = 200$ to $Cx = 201$. The incorrect mass flux by the interpolation-based schemes may lead to an inaccuracy in the computed value of the momentum input at the solid surface.

The reliability of the results obtained using the proposed OSIF and CPIF models can be evaluated by varying the location of the block center near the values of $Cx = 201$, 200, and 200.50, which denote the on-site and mid-plane BB schemes can be recovered, respectively, by using these positions, and thus the values are specified by $Cx = 200.01$, 200.49, 200.51, and 200.99. The corresponding results obtained for a Reynolds number of $Re = 165$ are presented in Table 1. It is clear that the numerical errors associated with the different block locations remain approximately stable. In other words, the proposed interpolation-free models yield results with a similar order of numerical error even when the values of $q$ are close to 1, 0 or 1/2. Thus, it is confirmed that both the OSIF and the CPIF models provide a stable and reliable mechanism for simulating curved boundary problems by LBM.

### 4.2. Application of curved boundary treatment models to moving boundary problems

In this section, the curved boundary treatments discussed above are extended to the simulation of moving boundary problems by adding the momentum effect described in Eq. (7) of Section 3 to the corresponding boundary model. The results presented in Section 4.1 have shown that the Bouzidi's and Yu's models have a very similar level of performance. Furthermore, it has been shown that the CPIF model provides more accurate results for the drag and lift forces acting on the block than the OSIF model. As a result, the moving curved boundary simulations discussed in this section of the paper are performed using the FH model, Bouzidi's linear interpolation model and the proposed CPIF model, respectively. The simulations commence by considering a square block moving at a constant velocity $u_{Wx}$ along the longitudinal axis (i.e. $x$-direction) of a 2D channel containing a stationary flow, and then consider the case of a circular cylinder moving along the same channel. To analyze the computational accuracy and test the Galilean invariance, the simulating

Fig. 6. Numerical results obtained by different curved boundary treatments for channel flow with stationary square block: (a1) variation of dimensionless drag force ($Fx^*$) with block center location for channel Reynolds number of $Re = 90$ (time-steps = 25,000); (a2) variation of dimensionless drag force ($Fx^*$) with block center location for channel Reynolds number of $Re = 165$ (time-steps = 30,000); (a3) variation of dimensionless drag force ($Fx^*$) with block center location for channel Reynolds number of $Re = 325$ (time-steps = 60,000); (b1) variation of lifting force ($Fy$) with time-steps computed by Yu's and Bouzidi's interpolation-based models for channel Reynolds number of $Re = 325$; (b2) variation of lifting force ($Fy$) with time-steps computed by FH model, and by the proposed OSIF/CPIF interpolation-free models for channel Reynolds number of $Re = 325$.

results in the cases of square/cylinder blocks traveling along the channel are then compared to the case of the Couette flow past the stationary square/cylinder blocks with identical sliding top/bottom walls velocity $u_{Wx}$ using the mid-plane BB scheme and the CPIF model, respectively.

In the initial simulations, it is assumed that the square block moves along the channel at a velocity corresponding to a block Reynolds number ($Re \equiv \frac{L \cdot u_{Wx}}{\nu}$) of either 10 or 40, respectively. The block is assumed to have a side-length of $L = 24$, the kinematic viscosity is determined by a relaxation factor of $\omega = 1.6$, and the block velocity $u_{Wx}$ is determined inversely from the specified block Reynolds number. In addition, the computational domain is mapped using a $1500 \times 100$ mesh and an assumption is made that the block center remains at $Cy = 50$ as it travels along the $x$-direction. The simulations of the Couette flow past the stationary square block with identical moving top/bottom walls velocity $u_{Wx}$ are then performed using the mid-plane BB scheme and CPIF model, respectively. The respective performances of the three curved boundary treatment schemes in the case of block traveling along the channel are evaluated by reference to the results of Couette flow obtained using a pure mid-plane BB scheme with no curved boundary treatment and CPIF model with the interpolation-free curved boundary treatment applied to the stationary square block, respectively.

Fig. 7 illustrates the variation of the calculated drag force $Fx$ over time for the cases where the square block travels with a velocity and the Couette flow with the identical sliding velocity corresponding to $Re = 10$. A momentum fluctuation effect is observed in all of the results for the moving block case, but particularly in those computed using Bouzidi's linear interpolation model. However, the average values of $Fx$ computed using the different models are broadly similar and agree with the reference value obtained by the mid-plane BB scheme and CPIF model in Couette flow case. The origins of the momentum fluctuation are well documented in [20], and hence are not discussed here. Fig. 8(a1) and (a2) presents the simulation results obtained by the various schemes for the drag force and the lift force, respectively, at a higher Reynolds number of $Re = 40$. It can be observed that, in the case of the Couette flow, the results of the drag/lift forces estimated by mid-plane BB scheme agree well with those evaluated by CPIF model as shown in Figs. 7 and 8(a1–a2), since the simple geometry of the square block induce less influence of the curved boundary treatment in computation. Fig. 8(a1) shows that the FH model, the Bouzidi linear interpolation model, and the proposed CPIF model all yield similar results in the case of block traveling along the channel for the drag force variation over time. The results for the lift force $Fy$ presented in Fig. 8(a2) shows that the use of an interpolation technique to treat the curved boundary in the moving block case induces the error fluid–solid interaction of momentum input at the solid–fluid interface. Fig. 8(b1) plots the vorticity contours computed by the four schemes in different flow cases (i.e. the block traveling along the channel and the Couette flow) after 20,000 time-steps. It can be seen that the results obtained using the FH model and the CPIF model in the moving block case are in good agreement. Furthermore, it is noted that the vorticity intensities computed by these two models are slightly

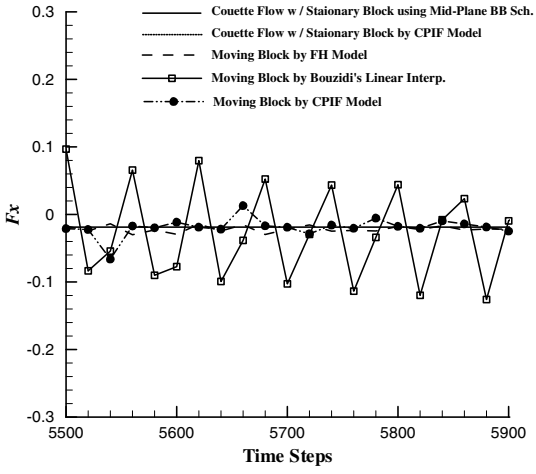


Fig. 7. Variation of drag force $Fx$ over time for square block moving within channel with block Reynolds number of $Re = 10$.

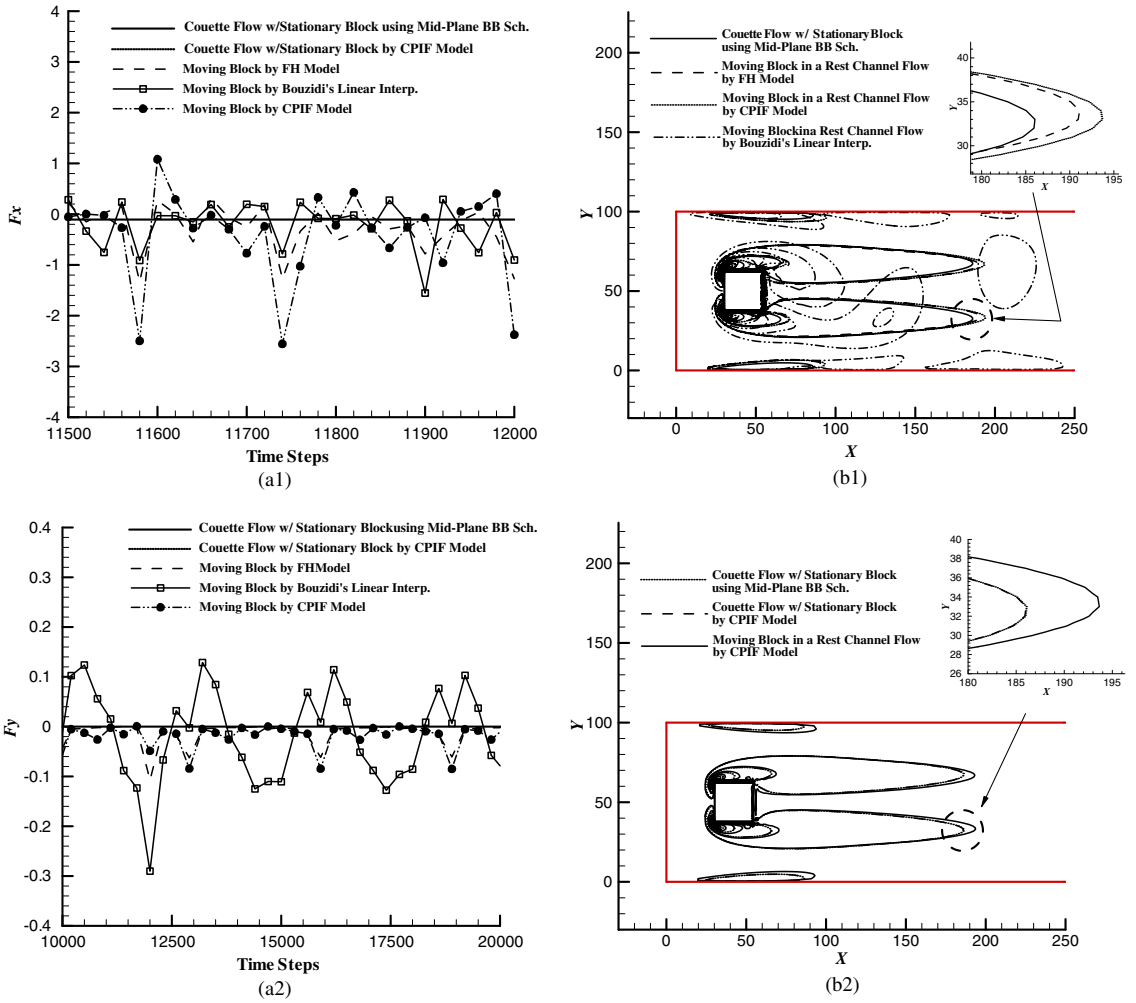


Fig. 8. Results obtained by various curved boundary schemes for square block moving within channel with block Reynolds number of $Re = 40$: (a1) variation of drag force $Fx$ over time; (a2) variation of lift force $Fy$ over time; (b1) vorticity contours at constant intensity level at time-step = 20,000; (b2) Galilean effect of the proposed CPIF model.

higher than those obtained from the pure mid-plane BB scheme with no curved boundary treatment in Couette flow with the stationary block at the corresponding Reynolds number. However, Bouzidi's linear interpolation-based model predicts the formation of a vortex shedding phenomenon characterized by asymmetric vorticity contours behind the moving block. This result suggests that the use of an interpolation-based curved boundary model induces an excessive perturbation of the flow field since interpolation breaks the mass conservation at the solid surface and therefore induces an error in the evaluated value of the momentum interaction. Furthermore, Fig. 8(b2) shows the vorticity contours computed by the CPIF model in the case of block traveling along the channel, and the vorticity contours solved by the mid-plane BB scheme and CPIF model, respectively, in the Couette flow problem. It is clear that the vorticity intensities in the Couette flow computed by BB and CPIF models are in good agreement but slightly lower than the results in the moving block case obtained using CPIF model. In the case of the block moving along the channel, a computational error can be produced when the extrapolations are applied to treat the nodes entering the fluid region from the solid region. However, applying the CPIF model for both moving block flow and the Couette flow, the differences of the results in the average drag/lift forces values and the vorticity contours between these two flow cases are no more than 5%. The Galilean invariance is therefore demonstrated.

Finally, the simulations consider the case of a circular cylinder traveling along the channel at a velocity corresponding to a cylinder Reynolds number of $Re \equiv \frac{D \cdot u_{Wx}}{\nu} = 40$. In performing the simulations, the cylinder is assumed to have a diameter of $D = 25$ and the relaxation factor is specified as $\omega = 1.6$, and the cylinder velocity $u_{Wx}$ is determined inversely from the specified cylinder Reynolds number. Furthermore, the Couette flow past the stationary cylinder with identical moving top/bottom walls velocity $u_{Wx}$ for the corresponding $Re = 40$ is also simulated by the mid-plane BB scheme and CPIF model, respectively.

Fig. 9(a1) and (a2) presents the corresponding simulation results for the drag force and the lift force, respectively. As in the case of the square block traveling along the channel, it is apparent in Fig. 9(a1) that the results obtained for the drag force using Bouzidi's linear interpolation model, the FH model, and the proposed CPIF model, respectively, are very similar for the case of the cylinder moving along the channel. It can also be seen that, in the Couette flow past the stationary cylinder, the results of drag force using a pure mid-plane BB scheme with no curved boundary treatment have near 6% departures from the drag force results obtained by the proposed CPIF model with curved boundary treatment, since a curved boundary treatment is necessary when simulating the flow past a circular cylinder. However, the lift force is found to be $Fy = 0$ both using the mid-plane BB scheme and the CPIF model in the Couette flow as shown in Fig. 8(a2). Therefore, it can be

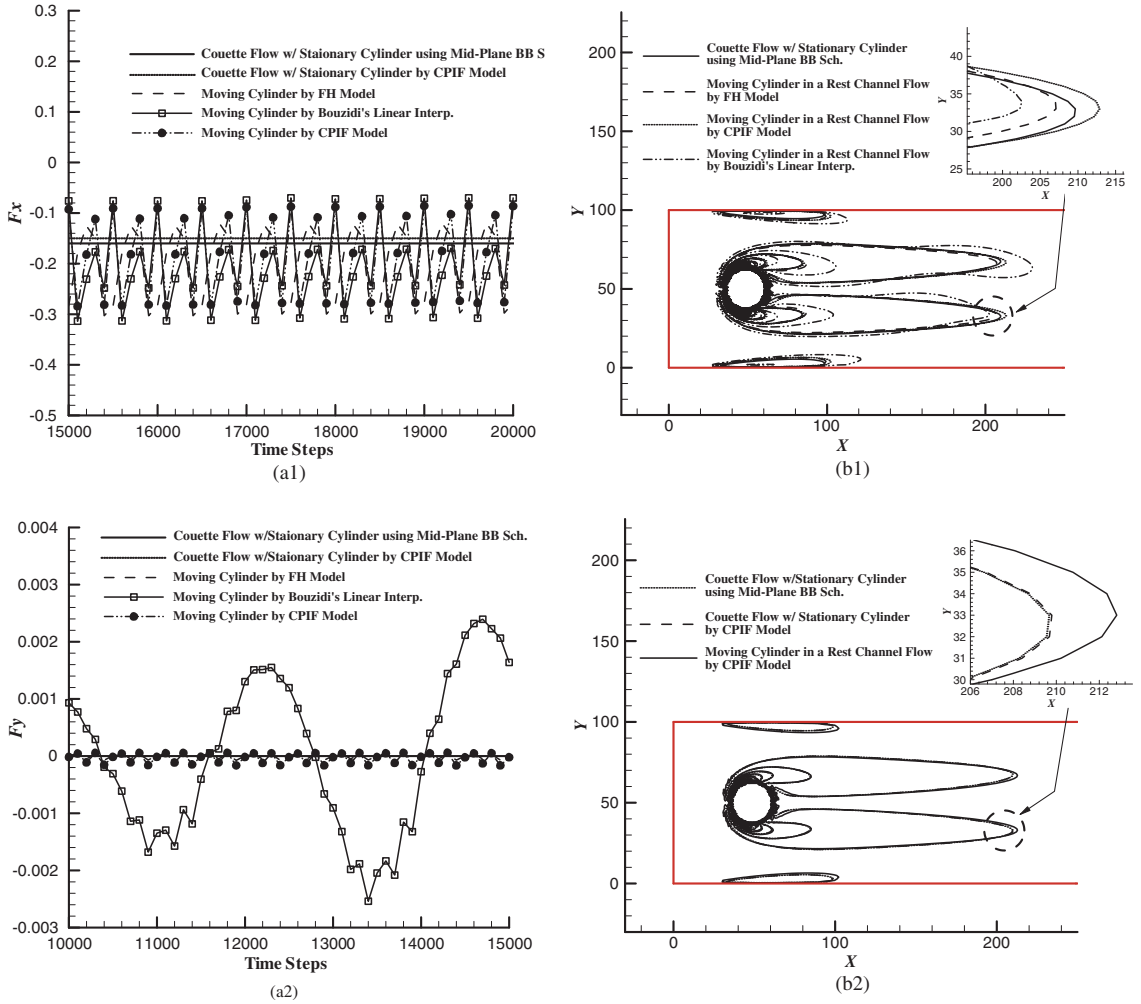


Fig. 9. Results obtained by various curved boundary schemes for circular cylinder moving within channel with cylinder Reynolds number of $Re = 40$: (a1) variation of drag force $Fx$ over time; (a2) variation of lift force $Fy$ over time; (b1) vorticity contours at constant intensity level at time-step = 21,000; (b2) Galilean effect of the proposed CPIF model.

inferred that a curved boundary treatment strategy yields a significant improvement in the computational accuracy compared to that obtained from the conventional stair-shaped curved approximation. However, the results for the lift force presented in Fig. 9(a2) shows that the use of an interpolation-based technique (e.g. Bouzidi's linear interpolation model) produces an error in the computed momentum input at the solid boundary. Finally, Fig. 9(b1) reveals that the pure mid-plane BB scheme, the FH model, and the CPIF model generate very similar results for the vorticity contours in the Couette flow and in the case of the cylinder moves along the channel, respectively. However, Bouzidi's model again predicts the formation of a vortex shedding effect behind the moving cylinder. As in the case of the moving square block, it is thought that this vortex shedding phenomenon can be attributed to an excessive perturbation of the momentum interaction as a result of the interpolation process. A small difference of the vorticity intensities obtained by the mid-plane BB scheme without curved boundary treatment and by the CPIF model with interpolation-free curved treatment in the Couette flow problem can be observed as shown in Fig. 9(b2). However, both the average drag/lift forces values and the vorticity contours solved by CPIF model in these two different flow cases, i.e. the moving cylinder case and the Couette flow past a stationary cylinder, exhibit the deviations less than 4% to demonstrate the Galilean invariance of the proposed CPIF model in present investigation.

## 5. Conclusion

This study has investigated the application of various curved boundary treatment schemes to the simulation of stationary and moving curved boundary problems. In addition, two interpolation-free schemes have been proposed based upon the FH local refinement treatment for grid transformation and two types of BB scheme, namely the on-site BB scheme (OSIF) and a composite (i.e. both on-site and mid-plane) BB scheme (CPIF). The resulting treatment procedure is independent of the collision step in LBM. The various curved boundary models have been applied in a series of simulations of 2D channel flow involving stationary or moving square blocks and a moving cylinder, respectively. In addition, a Couette flow past the stationary square/cylinder blocks with the moving top/bottom walls is simulated to test the Galilean invariance of the CPIF model. Overall, the numerical results have shown that the proposed interpolation-free schemes, i.e. the OSIF and CPIF models, reduce the mass flux error near the solid surface, and therefore yield a significant improvement in the computed value of the momentum input. Consequently, both models provide a suitable strategy for LB simulations of curved boundary applications. However, when the simulated system involves a moving curved boundary, the results have shown that the CPIF model provides more accurate results. The Galilean invariance is also demonstrated for the proposed CPIF model.

The current simulations have revealed the presence of spatial fluctuations in both the drag force and the lift force. The principal causes of this momentum fluctuation effect are discussed in [20], which indicated that two main sources of error exist. One is that the number of solid nodes changes as the square block or cylinder moves along the channel, and this has a direct impact on the computed value of the momentum transfer near the boundary surface. Furthermore, the treatment of the nodes entering the fluid region from the solid region of the computational domain is not unique, and the used extrapolations of treatment would cause the numerical errors somehow. Finally, it should be noted that even though the OSIF and CPIF models proposed in this study are intended to eliminate errors in the mass flux and momentum input, a minor mass non-conservation effect still inevitably exists because the modification of the unknown distribution functions near the curved boundary is required based upon a grid transformation technique. However, modification of the distribution function is confined to the non-equilibrium part (i.e. $f_i^{\mathrm{neq}}$) only. This part is far smaller than the equilibrium part, i.e. $f_i^{\mathrm{neq}} \ll f_i^{\mathrm{eq}}$, and therefore the effect of mass non-conservation is significantly reduced, with the result that the accuracy of the computed momentum interaction near the boundary is considerably improved.

The present study has developed simple interpolation-free models to overcome the drawbacks of conventional interpolation-based curved boundary treatments. The present results suggest that the application of interpolation techniques to compute the unknown distribution functions in LB simulations is not recommended. The distribution function is defined as the probability of particles number in phase-space with the specific momentum. The macroscopic flow properties, e.g. the flow density and momentum, are computed from the distribution functions in accordance with Eqs. (4a) and (4b). When interpolation is applied to solve the unknown distribution functions in LB simulations, e.g. as in Bouzidi's and Yu's models, both the

equilibrium and the non-equilibrium parts of the distribution functions are evaluated using an interpolation technique, which results in significant deviations of the macroscopic flow properties if the lattice (grid) size is not sufficiently small. In the FH model, the numerical accuracy of the simulation results may not be enhanced effectively by employing an additional collision step to solve the unknown distribution functions. However, the OSIF and CPIF models proposed in this study avoid the need for interpolation by modifying the non-equilibrium part of the unknown distribution functions in accordance with the principles of mass and momentum conservation and the need to ensure continuity of the deviatoric stress near the boundaries, respectively. The simulation results have confirmed that this approach effectively suppresses the problem of mass non-conservation at the solid–fluid interface and therefore improve the accuracy of the computational results considerably.

## References

[1] S. Chen, G. Doolen, Lattice Boltzmann method for fluid flows, Annu. Rev. Fluid Mech. 30 (1998) 329–364.
[2] D. Yu, R. Mei, L.S. Luo, W. Shyy, Viscous flow computations with the method of lattice Boltzmann equation, Progr. Aerospace Sci. 39 (2003) 329–367.
[3] D. Raabe, Overview of the lattice Boltzmann method for nano- and microscale fluid dynamics in materials science and engineering, Model. Simul. Mater. Sci. Eng. 12 (2004) R13–R46.
[4] S. Succi, The Lattice Boltzmann Equation for Fluid Dynamics and Beyond, Clarendon Press, Oxford, 2001.
[5] H. Yu, S.S. Girimaji, L.-S. Luo, DNS and LES of decaying isotropic turbulence with and without frame rotation using lattice Boltzmann method, J. Comput. Phys. 209 (2005) 599–616.
[6] H. Yu, L.-S. Luo, S.S. Girimaji, LES of turbulent square jet flow using an MRT lattice Boltzmann model, Comput. Fluids 35 (8/9) (2006) 957–965.
[7] O. Behrend, Solid boundaries in particle suspension simulations via lattice Boltzmann method, Phys. Rev. E 52 (1995) 1164–1175.
[8] A.J.C. Ladd, Numerical simulation of particular suspensions via discretized Boltzmann equation, Part 2. Numerical results, J. Fluid Mech. 271 (1994) 311–339.
[9] I. Ginzbourg, D. d'Humiéres, Local second-order boundary method for lattice Boltzmann models, J. Stat. Phys. 84 (1996) 927–971.
[10] L.S. Luo, Analytic solutions of linearized lattice Boltzmann equation for simple flow, J. Stat. Phys. 88 (1997) 913–926.
[11] X. He, Q. Zou, L.S. Luo, M. Dembo, Analytic solutions and analysis on no-slip boundary condition for the lattice Boltzmann BGK model, J. Stat. Phys. 87 (1997) 115–136.
[12] X. He, L.S. Luo, M. Dembo, Some progress in lattice Boltzmann method, Part 1. Non-uniform mesh grids, J. Comput. Phys. 129 (1996) 357–363.
[13] X. He, G. Doolen, Lattice Boltzmann method on a curvilinear coordinate system: vortex shedding behind a circular cylinder, Phys. Rev. E 56 (1997) 434–440.
[14] X. He, G. Doolen, Lattice Boltzmann method on curvilinear coordinates system: flow around a circular cylinder, J. Comput. Phys. 134 (1997) 306–315.
[15] O. Filippova, D. Hänel, Grid refinement for lattice-BGK models, J. Comput. Phys. 147 (1998) 219–228.
[16] R. Mei, L.S. Luo, W. Shyy, An accurate curved boundary treatment in the lattice Boltzmann method, J. Comput. Phys. 155 (1999) 307–330.
[17] R. Mei, W. Shyy, L.S. Luo, Lattice Boltzmann method for 3D flows with curved boundary, J. Comput. Phys. 161 (2000) 680–699.
[18] R. Mei, D. Yu, W. Shyy, L.S. Luo, Force evaluation in the lattice Boltzmann method involving curved geometry, Phys. Rev. E 65 (2002) 041203.
[19] M. Bouzidi, M. Firdaouss, P. Lallemand, Momentum transfer of a Boltzmann-lattice fluid with boundaries, Phys. Fluids 13 (11) (2001) 3452–3459.
[20] P. Lallemand, L.S. Luo, Lattice Boltzmann method for moving boundaries, J. Comput. Phys. 184 (2003) 406–421.
[21] D. Yu, R. Mei, W. Shyy, A unified boundary treatment in lattice Boltzmann method, AIAA 2003-0953, New York, 2003.
[22] Z.G. Feng, E.E. Michaelides, The immersed boundary-lattice Boltzmann method for solving fluid–particles interaction problems, J. Comput. Phys. 195 (2004) 602–628.
[23] Y. Peng, C. Shu, Y.T. Chew, X.D. Niu, X.Y. Lu, Application of multi-block approach in the immersed boundary-lattice Boltzmann method for viscous fluid flows, J. Comput. Phys. 218 (2006) 460–478.
[24] Y.H. Qian, D. d'Humieres, P. Lallemand, Lattice BGK models for Navier–Stokes equation, Europhys. Lett. 17 (6) (1992) 479–484.
[25] Y.H. Qian, S.A. Orszag, Lattice BGK models for the Navier–Stokes equation: non-linear deviation in compressible regimes, Europhys. Lett. 21 (1993) 255–259.
[26] C. Pan, L.S. Luo, C.T. Miller, An evaluation of the lattice Boltzmann schemes for porous medium flow simulation, Comput. Fluids 35 (2006) 898–909.
[27] P.-H. Kao, T.-F. Ren, R.-J. Yang, An investigation into fixed-bed microreactors using lattice Boltzmann method simulations, Int. J. Heat Mass Transf. 50 (2007) 4243–4255.
[28] H. Li, X. Lu, H. Fang, Y. Qian, Force evaluations in lattice Boltzmann simulations with moving boundaries in two dimensions, Phys. Rev. E 70 (2004) 026701.